

THE [O II] $\lambda 3727$ LUMINOSITY FUNCTION AT $Z \sim 1$ GUANGTUN ZHU¹, JOHN MOUSTAKAS¹, AND MICHAEL R. BLANTON¹*Draft version December 5, 2018*

ABSTRACT

We measure the evolution of the [O II] $\lambda 3727$ luminosity function at $0.75 < z < 1.45$ using high-resolution spectroscopy of $\sim 14,000$ galaxies observed by the DEEP2 galaxy redshift survey. We find that brighter than $L_{[\text{O II}]} = 10^{42} \text{ erg s}^{-1}$ the luminosity function is well-represented by a power law $dN/dL \propto L^\alpha$ with slope $\alpha \sim -3$. The number density of [O II]-emitting galaxies above this luminosity declines by a factor of $\gtrsim 2.5$ between $z \sim 1.35$ and $z \sim 0.84$. In the limit of no density evolution, the characteristic [O II] luminosity, defined as the luminosity where the space density equals $10^{-3.5} \text{ dex}^{-1} \text{ Mpc}^{-3}$, declines by a factor of ~ 1.7 over the same redshift interval. These results imply a $\sim 25\%$ per Gyr decrease in the amount of star formation in galaxies during this epoch. Integrating the observed [O II] luminosity function assuming a faint-end power-law slope of -1.3 ± 0.2 , we derive the integrated star formation rate density in four redshift bins centered around $z \sim 1$, and find that the evolution is consistent with previous measurements based on independent star formation rate indicators.

Subject headings: galaxies: evolution — galaxies: luminosity function — stars: formation

1. INTRODUCTION

Measuring the comoving space density of the star formation rate (SFR) as a function of cosmic epoch is one of the key issues concerning the study of galaxy formation and evolution. The current picture is that the star formation peaked at $z \sim 1 - 3$, and then declined by roughly an order-of-magnitude to the present day (see, e.g., Madau et al. 1996; Lilly et al. 1996; Hopkins 2004; Hopkins & Beacom 2006).

Among the most direct indicators of the instantaneous SFR in galaxies is the $\text{H}\alpha$ $\lambda 6563$ recombination line (Kennicutt 1983, 1992). $\text{H}\alpha$ can be observed in the optical in the local Universe (e.g., Gallego et al. 1995; Tresse et al. 1998; Kennicutt 2008). However, at $z \gtrsim 0.4$, it must be observed in the near infrared (e.g., Yan et al. 1999; Glazebrook et al. 1999; Hopkins et al. 2000; Tresse et al. 2002), or other less direct SFR indicators such as the [O II] $\lambda\lambda 3726, 3729$ doublet must be used.

Compared to $\text{H}\alpha$, [O II] is only indirectly coupled to the ionizing continuum from massive stars, and is more sensitive to variations in metal abundance, excitation, and dust attenuation. Nevertheless, because of its intrinsic strength and blue rest-frame wavelength, [O II] remains a good alternative SFR indicator for high-redshift galaxies (Kennicutt 1998; Jansen et al. 2001; Kewley et al. 2004; Moustakas & Kennicutt 2006). In the past decade, a number of investigators have measured the star formation rate density, ρ_{SFR} , at high redshift by studying the [O II] luminosity function (LF), either using spectroscopy (e.g., Hammer et al. 1997; Hogg et al. 1998; Gallego et al. 2002; Teplitz et al. 2003; Rigopoulou et al. 2005), or narrow-band imaging (e.g., Hippelein et al. 2003; Ly et al. 2007; Takahashi et al. 2007). Unfortunately, these studies have been hampered by small sam-

ple size, small volume probed, and an inconsistent treatment of dust obscuration. Methods like narrow-band imaging also suffer from difficulties in continuum subtraction and contamination from other emission lines.

To circumvent these issues, we measure the [O II] luminosity function at $z \sim 1$ using data from the Deep Extragalactic Evolutionary Probe II survey (DEEP2²; Davis et al. 2003). DEEP2 has obtained high-resolution spectra for $\sim 50,000$ objects over four separate fields, making it the largest existing spectroscopic redshift survey of galaxies at these redshifts. We use these data to measure the [O II] luminosity function in four redshift bins at $0.75 < z < 1.45$.

In §2, we briefly describe our sample and the method used to calculate the LF. In §3 and §4 we present the observed [O II] LF and its evolution with redshift, respectively. Finally, in §5, we compute ρ_{SFR} in several redshift bins centered on $z \sim 1$, and we summarize our principal conclusions in §6.

Throughout this work, we adopt a Λ CDM cosmology with $\Omega_m = 0.3$, $\Omega_\Lambda = 0.7$ and $H_0 = 70 \text{ km s}^{-1} \text{ Mpc}^{-1}$. All magnitudes are on the AB system.

2. DATA AND METHOD

2.1. Data: DEEP2 DR3

We select our sample from the DEEP2 third public data release (DR3), which includes *BRI* photometry and spectra for $\sim 50,000$ galaxies in four widely separated fields. The high-resolution ($R \equiv \lambda/\delta\lambda \sim 5000$) spectra, which were acquired using the Keck-II/DEIMOS spectrograph (Faber et al. 2003), span two wavelength ranges, $6525 - 7825 \text{ \AA}$ and $7855 - 9120 \text{ \AA}$. Consequently, [O II] is measurable for objects in the following two redshift ranges, $0.752 < z < 1.099$ and $1.108 < z < 1.446$. Below, to study the evolution of the [O II] LF, we further split each bin into two additional redshift bins. We refer the reader to Davis et al. (2003), Coil et al. (2004),

¹ Center for Cosmology and Particle Physics, Department of Physics, New York University, 4 Washington Place, New York, NY 10003, gz323@nyu.edu, john.moustakas@nyu.edu, michael.blanton@nyu.edu

² <http://deep.berkeley.edu>

and Davis et al. (2007) for additional details regarding the DEEP2 survey.

In addition to the flux cut, $R < 24.1$ mag, the DEEP2 team applied the following color cuts to preselect galaxies at $z > 0.7$ in Fields 2, 3, and 4:

$$\begin{aligned} B - R &< 2.35(R - I) - 0.25 \text{ or;} \\ R - I &> 1.15 \text{ or;} \\ B - R &< 0.50. \end{aligned} \quad (1)$$

In the Extended Groth Strip (EGS, Field 1), to test their sample preselection method, the DEEP2 team did not apply the BRI color cuts. However, in order to make all four fields consistent, here we apply the color cuts given by equation (1) to the redshift and photometric catalogs in the EGS field. We apply additional angular cuts to avoid survey edges and to exclude gaps in the spectroscopy. Our final catalog contains 36,118 objects, of which 24,739 have accurate redshifts (quality $Q = 3$ or 4 as defined by Davis et al. 2007). The areas of the four fields are 0.38, 0.56, 0.88 and 0.63 deg², respectively, and the total area is 2.45 deg².

The DEEP2 spectra are not flux-calibrated; therefore, we infer the [O II] luminosity from the emission-line equivalent width (EW), which is insensitive to fluxing issues. We model each component of the [O II] $\lambda\lambda 3726, 3729$ doublet simultaneously using two Gaussian profiles, constraining the wavelength separation and velocity width, deconvolved for the instrumental resolution, to be identical. We then measure the continuum flux around each line and divide the integrated line flux by the local continuum to construct the EW. To estimate the continuum luminosity around [O II] we fit the broadband BRI photometry using the `deep_kcorrect` routine of `kcorrect`³ (v4.1.4; Blanton & Roweis 2007) and interpolate the best-fitting spectral energy distribution (SED) at 3727 Å. Above $z \sim 1.2$ the effective wavelength of the I -band bandpass falls blueward of 3700 Å; therefore, this technique does involve some extrapolation of the model for our highest redshift bin. Finally, we multiply the rest-frame EW by the luminosity of the continuum to infer the integrated emission-line luminosity. Note that this technique has the advantage that it automatically accounts for aperture effects, assuming that the relative intensity of star formation and stellar light inside and outside the slit does not vary significantly. Hereafter, we combine the two components of the [O II] doublet and consider the total [O II] $\lambda 3727$ emission-line luminosity.

Our [O II] measurement technique is similar to that used by the DEEP2 team (Weiner et al. 2007; Cooper et al. 2008), although the procedures used to compute K -corrections are totally independent. A comparison of our measurements shows no systematic differences and a $\sim 25\%$ scatter, which is comparable to the typical measurement error. We also checked our work by replacing our measurements with theirs, and obtained consistent results. In the following analysis we use our measurements.

We consider an [O II] measurement with signal to noise ratio (S/N) larger than 5 as reliable. In detail, our results are not sensitive to the specific S/N cut used since it only affects weak [O II] detections, for which we are

incomplete anyway. For example, using $S/N > 2$ has no significant effect on our conclusions. Our final sample of [O II]-emitting galaxies contains 13,726 objects.

2.2. Method: $1/V_{\max}$ Method

To calculate the luminosity function, we use the non-parametric $1/V_{\max}$ method. For a given galaxy, we calculate:

$$V_{\max} = \frac{1}{3} \int d\Omega \int_{z_{\min}}^{z_{\max}} dz \frac{d[D_c(z)^3]}{dz} f(z), \quad (2)$$

which is suitable for a spatially flat universe. The angular integral is limited to the DEEP2 area, $D_c(z)$ is the comoving distance as defined by Hogg (1999), and $f(z)$ expresses the probability of selecting each galaxy in our sample. We assume that $f(z)$ is given by the product of three quantities: $f = f_{\text{target}} \times f_{\text{success}} \times f_{\text{cut}}$, where f_{target} is the rate at which a source of a given R -band magnitude and $B - R$ and $R - I$ color was targeted [see eq. (1)], f_{success} is the rate at which a redshift was successfully measured, and f_{cut} is a step function, which we determined using the BRI magnitudes and the [O II] S/N , as described below. We experimented with including the surface brightness as a fourth variable in the completeness function (see, e.g., Lin et al. 2008), but found that it did not significantly affect our measured LFs. Since including a fourth dimension would introduce unnecessary scatter, we chose to construct the completeness function from just R , $R - I$, and $B - R$.

For a given galaxy, we calculate V_{\max} using a Monte Carlo method (see Blanton 2006). We randomly choose 1200 values of redshift z between z_{\min} and z_{\max} , uniformly distributed in volume. For each redshift, we calculate what the magnitudes of the object would be using `deep_kcorrect`. To estimate the [O II] S/N at each mock redshift, we first determine the mean noise spectrum for every DEEP2 mask. Then, for a given galaxy, we randomly choose a mask and the corresponding noise spectrum and compare the noise at the actual observed wavelength of [O II] to that at the simulated wavelength as if the galaxy were at the simulated redshift, and obtain the new S/N . We then apply the appropriate flux cut, color cuts, [O II] S/N cut and the completeness function to determine the fraction of mock sources that would have passed our selection criteria. Finally, V_{\max} is given by the volume multiplied by this fraction.

When determining the completeness function, we assume a 100% success rate for blue galaxies; that is, we assume that the only targetted blue galaxies without successfully measured redshifts are those for which [O II] falls outside the wavelength range of the spectra, and thus outside the redshift range studied here. Here, we have defined blue galaxies using the same definition as Willmer et al. (2006), who also made the same assumption regarding blue galaxies without well-measured redshifts. This assumption is especially reasonable in our analysis because a well-detected [O II] doublet will always result in a well-measured redshift. Finally, we tested our completeness function by calculating the B -band LF for all galaxies and comparing with Willmer et al. (2006), and found excellent statistical agreement, and no systematic differences.

3. THE OBSERVED [O II] LUMINOSITY FUNCTION

³ <http://cosmo.nyu.edu/blanton/kcorrect>

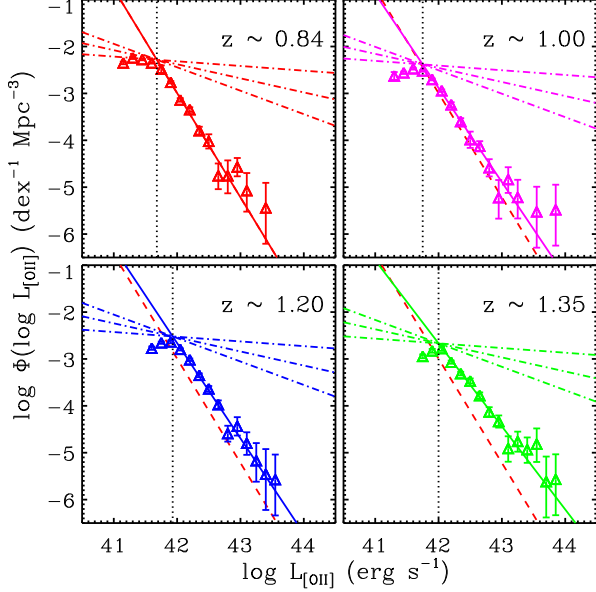


FIG. 1.— Observed [O II] luminosity function in four redshift bins. The solid lines are the power law fits to the bright part of the luminosity function. The dashed lines in the three highest redshift bins correspond to the solid line in the top-left panel. The three dashed-dotted lines correspond to three different faint-end slopes, -1.1 , -1.3 and -1.5 , and the dotted lines in each panel indicate the *turnover* in the luminosity function.

We measure the [O II] luminosity function in four redshift bins: $0.752 < z < 0.926$, $0.926 < z < 1.099$, $1.108 < z < 1.277$ and $1.277 < z < 1.446$, according to where the [O II] doublet can be measured reliably in the DEEP2 spectra. The median redshifts of the [O II]-emitting galaxies within these four redshift bins are 0.836, 1.002, 1.194, and 1.346, containing 5338, 3845, 2814 and 1729 galaxies in each bin, respectively.

The resulting [O II] LFs are tabulated in Table 1 and illustrated in Figure 1. The error bars shown in the figure are 84.13% confidence Poisson upper limits and lower limits estimated using the approximate formulae given by Gehrels (1986) [see eqs. (10) and (14) in that paper]. The distribution of the LF must follow a scaled Poisson distribution. To determine the scaling factor, within each luminosity bin, we define the effective weight (W_{eff}) by:

$$W_{\text{eff}} = \left[\sum_i \frac{1}{(V_{\text{max}})_i^2} \right] / \left[\sum_i \frac{1}{(V_{\text{max}})_i} \right], \quad (3)$$

and the effective number (N_{eff}) of objects by:

$$N_{\text{eff}} = \left[\sum_i \frac{1}{(V_{\text{max}})_i} \right] / W_{\text{eff}}. \quad (4)$$

We then calculate the upper limit and lower limit for the effective number, and multiply them by the effective weight to obtain the upper limit and lower limit for the luminosity density in each bin. For comparison, the square root Poisson error gives:

$$\sigma_{\Phi} = \sqrt{N_{\text{eff}}} W_{\text{eff}} = \sqrt{\sum_i \frac{1}{(V_{\text{max}})_i^2}}, \quad (5)$$

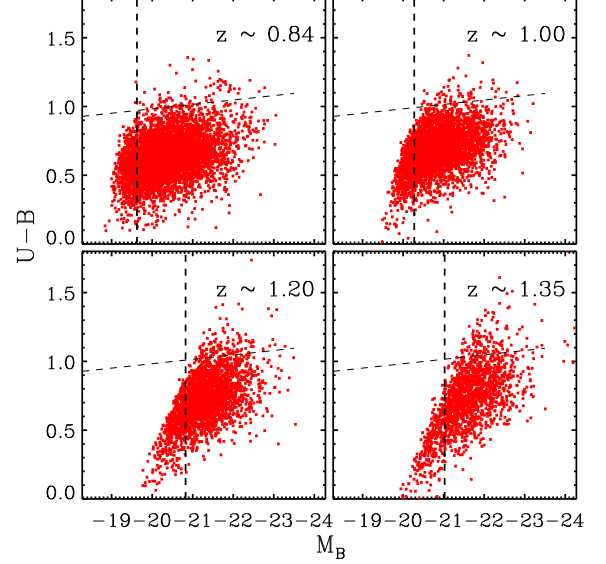


FIG. 2.— Rest-frame color-magnitude diagrams. The thin dashed lines show the division between blue galaxies and red galaxies (see Willmer et al. 2006), and the thick dashed lines show the approximate M_B completeness limit for our sample.

which is commonly used in the literature. The Poisson errors, however, do not include the effects of cosmic variance. Since we have four widely separated fields, we determine the error due to cosmic variance, σ_{cv} , by calculating the variance among the four independent fields, and list the results in Table 1.

Examining Figure 1, the commonly used Schechter (1976) function is clearly not a good representation of the data. Instead, we model the observed [O II] LF in each redshift bin as a power law:

$$\Phi(\log L)d(\log L) = 10^{(\alpha+1)(\log L - 42.5) + \beta} d(\log L), \quad (6)$$

where L is $L_{[\text{OII}]}$ in erg s^{-1} , and α and β are dimensionless parameters. We find the best fitting parameters (α, β) using a non-linear least square fit to the [O II] LFs weighted by the average Poisson errors. These parameters are presented in Table 2. Our results show that the bright part of each LF can be represented by a power law $dN/dL \propto L^\alpha$ with slope $\alpha \sim -3$. The slope for the highest redshift bin is the flattest: -2.77 ± 0.12 . However, it is possible that the LF in this bin may be underestimated due to incompleteness (see below).

Unfortunately, we are unable to constrain the faint end of the [O II] LF, especially in the highest redshift bin. To analyze the completeness, and in particular to test the significance of the observed *turnover* (TO) in the LF (*vertical dotted lines*; Fig. 1), we construct two diagnostic diagrams. In Figure 2 we show the $U-B$ versus M_B color-magnitude diagram for our sample. We plot the approximate B -band completeness limits for blue galaxies as dashed lines, where the sloping color cut has been defined by Willmer et al. (2006), and the thick vertical dashed line roughly corresponds to where the data and the color cut begin to deviate. In Figure 3 we plot the density distribution of points in the $M_B - \log(L_{[\text{OII}]})$ plane in grey scale; the two contours enclose 50% and

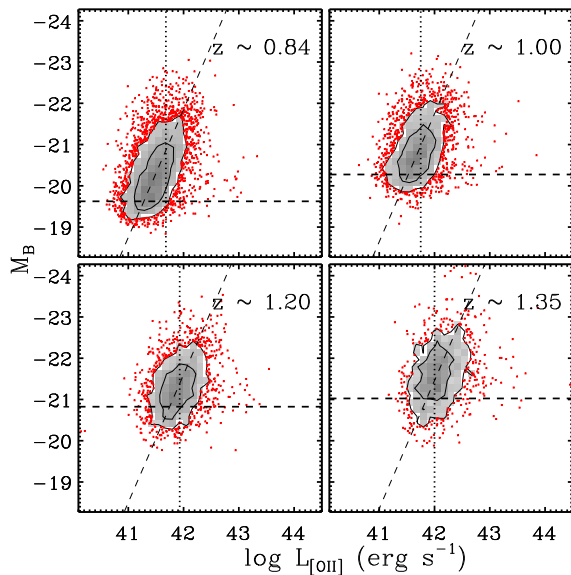


FIG. 3.— $M_B - \log(L_{[\text{OII}]})$ distribution. The dotted lines are the same as in Figure 1. The thick dashed lines show the M_B approximate completeness limit for blue galaxies (see Figure 2). The thin dashed lines have a slope of $-3.1 \text{ mag dex}^{-1}$, and show the approximate median relation between M_B and $\log(L_{[\text{OII}]})$.

80% of the points, respectively. The thin dashed lines in this figure all have a slope of $-3.1 \text{ mag dex}^{-1}$. This slope is formally consistent with performing a mean ordinary least squares fit to the data (Isobe et al. 1990). For our purposes, we note that the line roughly bisects the distribution of points in each panel, i.e., it approximates the median relation between $L_{[\text{OII}]}$ and M_B . The thick horizontal dashed lines in each panel are equivalent to the thick vertical dashed line plotted in the respective panels in Figure 2, and the vertical dotted lines give the position of the turnover in the respective [O II] LF (Fig. 1). The majority of the galaxies missing from our sample should be along and to the left of the thin dashed line.

Figure 3 demonstrates that, brighter than the turnover, we expect the sample to be complete because the majority of the unobserved galaxies below the M_B completeness limit are along and to the left of the thin dashed line. Fainter than the turnover, the sample becomes increasingly incomplete. In the two lowest redshift bins, the turnovers appear to be significant, because fainter than the turnover the difference between the measured LF and the extrapolation of the power law fitted to the bright part of the LF is so significant that it is unlikely to be due to incompleteness. In the two highest redshift bins, however, because the M_B completeness limit is very bright, it is possible that the turnovers are artificial, caused by the incompleteness of the survey. In the highest redshift bin, the M_B completeness limit is so bright that the slope of the LF may be even steeper than we have derived.

To summarize, we are unable to constrain the faint end of the [O II] luminosity function. However, we emphasize that the evolutionary analysis presented in §4 is unaffected by our ignorance of the faint end, because we restrict our analysis to the bright part of the [O II] LF

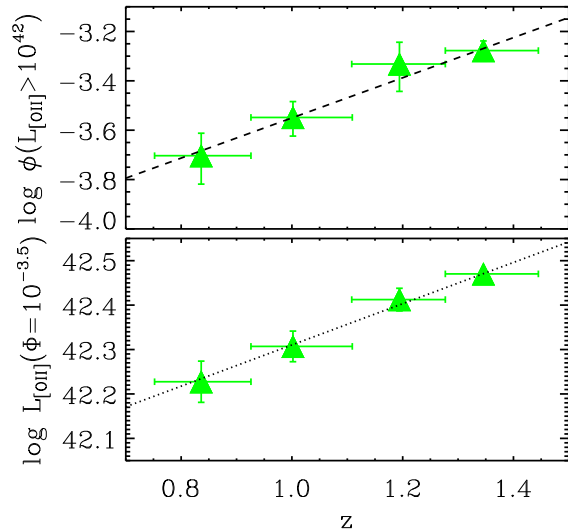


FIG. 4.— Evolution of the [O II] luminosity function. (Top) Evolution of the total number density in Mpc^{-3} of the strongest [O II]-emitting galaxies with $L_{[\text{OII}]} > 10^{42} \text{ erg s}^{-1}$. The dashed line is the linear fit to the data given by eq. (7). (Bottom) Evolution of the characteristic luminosity, in erg s^{-1} , defined by where the space density of [O II]-emitting galaxies equals $10^{-3.5} \text{ dex}^{-1} \text{ Mpc}^{-3}$. The dotted line is the linear fit to the data given by eq. (8).

where we are statistically complete. In §5, when integrating the [O II] LF to obtain an estimate of the SFR density, we do make some simplifying assumptions regarding the form of the faint end of the LF.

4. THE EVOLUTION OF THE [O II] LUMINOSITY FUNCTION

The uncertainty in the faint end of the [O II] LF prevents us from obtaining a reliable estimate of the total [O II] luminosity density. Therefore, we focus instead on the integrated number density, $\phi \equiv \int_L^\infty \Phi(L) dL$, of the strongest [O II]-emitting galaxies. Assuming that the turnover luminosity in the highest redshift bin is $\leq 10^{42} \text{ erg s}^{-1}$, we integrate our model of the LF in each redshift bin over $L_{[\text{OII}]} > 10^{42} \text{ erg s}^{-1}$, and present the results in the top panel of Figure 4 and in Table 2. The horizontal error bars indicate the range of each redshift bin, and the vertical error bars are given by the cosmic variance among the four fields, which dominate the error budget. We find that the total number density of the strongest [O II]-emitting galaxies, i.e., those with $L_{[\text{OII}]} > 10^{42} \text{ erg s}^{-1}$, declines by a factor of $\gtrsim 2.5$ between $z \sim 1.35$ and $z \sim 0.84$. A linear fit to the four points gives a slope of ~ 0.8 :

$$\log [\phi(L_{[\text{OII}]} > 10^{42} \text{ erg s}^{-1})] = a z - b, \quad (7)$$

with $(a, b) = (0.81 \pm 0.16, -4.36 \pm 0.19)$ and $\phi(L_{[\text{OII}]} > 10^{42} \text{ erg s}^{-1})$ in Mpc^{-3} . This fit is shown as the dashed line in Figure 4.

The observed decrease in the number density of [O II]-emitting galaxies may be caused by the decline of the overall number density of galaxies in the universe, but also may be driven by the evolution of the luminosity

function itself. We attempt to constrain the amount of evolution by measuring the luminosity at a fixed space density (see, e.g., Brown et al. 2007). We define a characteristic luminosity where the space density equals $10^{-3.5} \text{ dex}^{-1} \text{ Mpc}^{-3}$, which has the advantage that it is independent of the faint end of the LF. We show the characteristic luminosity as a function of redshift in the bottom panel of Figure 4, and list the results in Table 2. Once again, the vertical error bars are dominated by cosmic variance. We find that the characteristic luminosity has declined by a factor of ~ 1.7 between $z \sim 1.35$ and $z \sim 0.84$. We perform a linear fit to the four points and obtain a slope of ~ 0.5 :

$$\log [L_{[\text{O II}]}(\Phi = 10^{-3.5} \text{ dex}^{-1} \text{ Mpc}^{-3})] = c z + d, \quad (8)$$

with $(c, d) = (0.46 \pm 0.07, 41.85 \pm 0.09)$ and $L_{[\text{O II}]}$ in erg s^{-1} . The resulting fit is shown as the dotted line in Figure 4.

Unfortunately, we are unable to perform a detailed comparison of our results with previously published measurements of the [O II] LF, in part because previous studies have relied on considerably smaller samples (e.g., samples of $10 - 1000$ objects) over much smaller areas (e.g., $10' \times 10'$ in Hippelein et al. 2003). Consequently, existing measurements of the [O II] LF at $z \sim 1$ have large uncertainties at the bright end, and suffer from large uncertainties due to cosmic variance, which we have shown are the dominant significant source of uncertainty. Nevertheless, to the extent we can make simple comparisons, we find that our results agree with previous studies reasonably well. For example, interpolating the [O II] LFs published by Hogg et al. (1998), Teplitz et al. (2003), Hippelein et al. (2003), Ly et al. (2007) at $z \sim 1$ gives $\log[L_{[\text{O II}]}(\Phi = 10^{-3.5})] \sim 42.0 - 42.5$, which agrees reasonably well with what we have found.

To summarize, we find that the total number density of the strongest [O II]-emitting galaxies has declined by a factor of $\gtrsim 2.5$ between $z \sim 1.35$ and $z \sim 0.84$, when the Universe aged from 4.6 Gyr to 6.4 Gyr. This decline may be driven by a decline in the overall number density of galaxies in the Universe, or by a fading of the [O II] LF. Unfortunately, we are unable to establish whether number-density evolution, luminosity evolution, or a combination of both is responsible for the observed evolution. If luminosity evolution is the dominant driver of the change in the [O II] LF over $0.84 < z < 1.35$, and the [O II] luminosity is proportional to star formation rate (see §5), then our results imply that the SFR in galaxies declined by $\sim 25\%$ per Gyr during this epoch.

5. THE EVOLUTION OF THE STAR FORMATION RATE DENSITY

Converting the observed [O II] luminosity into a SFR is subject to considerable random and systematic uncertainties, arising from variations in dust attenuation, metallicity, and excitation among star-forming galaxies (Kennicutt 1992; Jansen et al. 2001; Kewley et al. 2004; Moustakas et al. 2006). In a recent analysis, Moustakas et al. (2006) have shown that dust reddening, as derived using the $\text{H}\alpha/\text{H}\beta$ Balmer decrement, is responsible for the bulk of the scatter in [O II] as a SFR indicator, while variations in metallicity and excitation

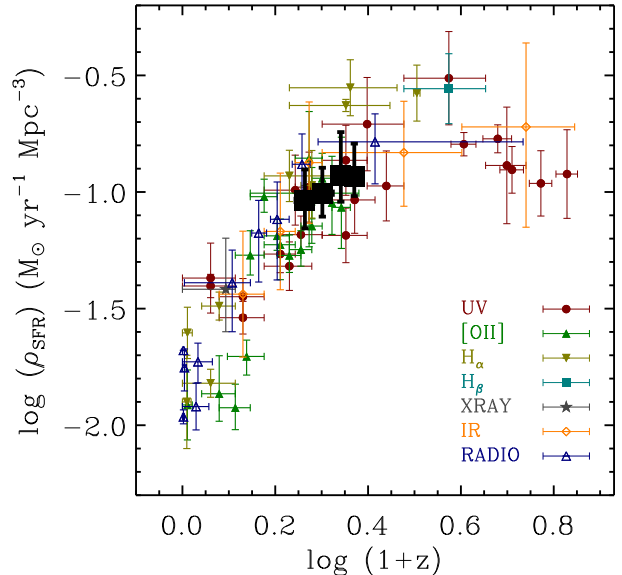


FIG. 5.— SFR density, ρ_{SFR} , versus redshift based on various multi-wavelength SFR indicators (Hopkins 2004). Our four estimates of ρ_{SFR} are shown as large filled squares, where the vertical error bars are obtained by allowing the turnover positions and the slope of the faint end of the [O II] luminosity function to vary in a sensible way (see text for details).

are second-order effects for most galaxies. Another potential concern is that the [O II] emission might be arising from an active galactic nucleus (AGN) rather than star formation. However, based on the properties of local galaxies (e.g., Kauffmann et al. 2003), our sample of luminous blue galaxies are unlikely to be hosting powerful AGN that would dominate the integrated line-emission; moreover, the fraction of sources with broad [O II] emission ($> 500 \text{ km s}^{-1}$ FWHM) is $\ll 0.1\%$. Therefore, we conclude that AGN contamination is a negligible source of error on our results.

In the absence of an estimate of the Balmer decrement, Moustakas et al. (2006) recommend using an empirically derived correlation between the absolute B -band magnitude, and the $L_{[\text{O II}]}$ /SFR ratio, where the SFR is in $\text{M}_{\odot} \text{ yr}^{-1}$. This calibration removes the gross systematic effects of reddening, metallicity, and excitation, and has been shown to work reasonably well for star-forming galaxies to $z \approx 1$ (Moustakas et al. 2006; Cooper et al. 2008). Instead of using the B -band luminosity of each individual galaxy, we obtain a statistical estimate of M_B for each object from $L_{[\text{O II}]}$ using the thin dashed line in Figure 3. We then calculate the appropriate $L_{[\text{O II}]}$ /SFR conversion factor by interpolating Table 2 in Moustakas et al. (2006) to derive the SFR.

Before integrating the observed [O II] LF to derive the SFR density, ρ_{SFR} , we must make some assumptions regarding the form of the faint end of the LF (see §3). First, we allow the luminosity of the turnover in the LF in each redshift bin to vary over a sensible range of values to account for the uncertainties in our completeness. Specifically, for the two lowest redshift bins, we assume

$\log(L_{\text{TO}}) = 41.68 \pm 0.10$ and 41.75 ± 0.10 erg s $^{-1}$, respectively, while for the two highest redshift bins, we adopt a fainter lower limit: $\log(L_{\text{TO}}) = 41.93^{+0.10}_{-0.20}$ and $42.00^{+0.10}_{-0.20}$ erg s $^{-1}$.

Second, we must assume a form for the [O II] LF fainter than the turnover luminosity. Previous studies (e.g. Gallego et al. 2002; Ly et al. 2007) have assumed that the [O II] LF is a Schechter (1976) function, which is a power-law in the faint end. However, the faint-end slope, α_{faint} , is usually not well-constrained. Consequently, hereafter we allow α_{faint} to vary between -1.1 and -1.5 , which brackets the value, $\alpha_{\text{faint}} = -1.3 \pm 0.2$, that we measure from the lowest redshift bin in Figure 1. For comparison, Willmer et al. (2006) assumed a faint-end slope of -1.3 for the B -band LF of blue galaxies at $0.3 < z < 1.3$.

To summarize, we assume that the [O II] luminosity function is a double power-law with slope:

$$\begin{cases} \alpha_{\text{faint}} = -1.3 \pm 0.2 & \text{for } L_{[\text{OII}]} < L_{\text{TO}} \\ \alpha & \text{for } L_{[\text{OII}]} \geq L_{\text{TO}} \end{cases}$$

where α is derived from our fit to the bright part of the LF where we are complete. Given these assumptions, we integrate the observed LFs and list the results in Table 2.

Figure 5 compares our measurements of ρ_{SFR} at $z \sim 1$ against a large compilation of multi-wavelength measurements from the literature by Hopkins (2004). Our results agree remarkably well with these independent measurements considering the uncertainties in converting $L_{[\text{OII}]}$ into a SFR, and our incompleteness at the faint end of the LF.

6. CONCLUSIONS

Because its blue rest-frame wavelength and intrinsic strength allow it to be measured up to $z \sim 1.6$ in the optical, the [O II] $\lambda\lambda 3726, 3729$ doublet plays a unique role in the study of galaxy evolution. We have used spectroscopy of $\sim 14,000$ galaxies from the DEEP2 galaxy redshift survey to measure the [O II] luminosity function at $0.75 < z < 1.45$. Our sample is orders-of-magnitude larger than previous spectroscopic studies, over a considerable larger area spanning four independent fields, allowing us to minimize the systematic effects of cosmic variance. Our principal results are given in Tables 1 and 2, and illustrated in Figures 1 and 4. We found that the bright part of the [O II] LF is well-represented by

a power-law $dN/dL \propto L^\alpha$ with slope $\alpha \sim -3$. However, survey incompleteness prevented us from constraining the faint end of the LF.

We measured the evolution of the [O II] LF using two quantities that only rely on the bright part of the [O II] LF where we are statistically complete. First, we calculated the total number density of galaxies with $L_{[\text{OII}]} > 10^{42}$ erg s $^{-1}$, and found that it has declined by a factor of $\gtrsim 2.5$ between $z \sim 1.35$ and $z \sim 0.84$. Second, we calculated the characteristic luminosity, the luminosity where the space density of [O II]-emitting galaxies equals $10^{-3.5}$ dex $^{-1}$ Mpc $^{-3}$, and found that it has declined by a factor of ~ 1.7 over the same redshift interval. Assuming that the [O II] luminosity is proportional to the SFR, these results imply that the SFR in galaxies declined by $\sim 25\%$ per Gyr during this epoch.

Finally, we used the empirical calibration between $L_{[\text{OII}]}$ and SFR published by Moustakas et al. (2006), and adopted some simple assumptions regarding the faint end of the [O II] LF, to obtain an estimate of the integrated SFR density, ρ_{SFR} , in four redshift bins centered around $z \sim 1$. We found that, despite the considerable uncertainties, the evolution we measure is consistent with previous measurements based on a variety of independent, multi-wavelength SFR indicators.

It is a pleasure to thank Jeffrey A. Newman and David W. Hogg for numerous comments that helped improve the manuscript, and Benjamin J. Weiner for sharing his [O II] measurements for comparison.

Funding for the DEEP2 survey has been provided by NSF grants AST95-09298, AST-0071048, AST-0071198, AST-0507428, and AST-0507483 as well as NASA LTSA grant NNG04GC89G.

Some of the data presented herein were obtained at the W. M. Keck Observatory, which is operated as a scientific partnership among the California Institute of Technology, the University of California and the National Aeronautics and Space Administration. The Observatory was made possible by the generous financial support of the W. M. Keck Foundation. The DEEP2 team and Keck Observatory acknowledge the very significant cultural role and reverence that the summit of Mauna Kea has always had within the indigenous Hawaiian community and appreciate the opportunity to conduct observations from this mountain.

REFERENCES

- Blanton, M. R., et al. 2006, ApJ, 648, 268
 Blanton, M. R., & Roweis, S. 2007, AJ, 133, 734
 Brown, M. J. J., et al. 2007, ApJ, 654, 858
 Coil, A. L., et al. 2004, ApJ, 617, 765
 Cooper, M. C., et al. 2008, MNRAS, 383, 1058
 Davis, M., et al. 2003, Proc. SPIE, 4834, 161
 Davis, M., et al. 2007, ApJ, 660, L1
 Faber, S. M., et al. 2003, Proc. SPIE, 4841, 1657
 Gallego, J., Zamorano, J., Aragón-Salamanca, A., & Rego, M. 1995, ApJ, 455, L1
 Gallego, J., García-Dabó, C. E., Zamorano, J., Aragón-Salamanca, A., & Rego, M. 2002, ApJ, 570, L1
 Gehrels, N. 1986, ApJ, 303, 336
 Glazebrook, K., Blake, C., Economou, F., Lilly, S., & Colless, M. 1999, MNRAS, 306, 843
 Hammer, F., et al. 1997, ApJ, 481, 49
 Hippelein, H., et al. 2003, A&A, 402, 65
 Hogg, D. W., Cohen, J. G., Blandford, R., & Pahre, M. A. 1998, ApJ, 504, 622
 Hogg, D. W. 1999, arXiv:astro-ph/9905116
 Hopkins, A. M., Connolly, A. J., & Szalay, A. S. 2000, AJ, 120, 2843
 Hopkins, A. M. 2004, ApJ, 504, 622
 Hopkins, A. M., & Beacom, J. F. 2006, ApJ, 651, 142
 Isobe, T., Feigelson, E. D., Akritas, M. G., & Babu, G. J. 1990, ApJ, 364, 104
 Jansen, R. A., Franx, M., & Fabricant, D. 2001, ApJ, 551, 825
 Kauffmann, G. et al. 2003, MNRAS, 346, 1055
 Kennicutt, R. C. 1983, ApJ, 272, 54
 Kennicutt, R. C. 1992, ApJ, 388, 310
 Kennicutt, R. C. 1998, ARA&A, 36, 189
 Kennicutt, R. C. 2008, ApJS, 178, 247
 Kewley, L. J., Geller, M. J., & Jansen, R. A. 2004, AJ, 127, 2002
 Lilly, S. J., Le Fevre, O., Hammer, F., & Crampton, D. 1996, ApJ, 460, L1

- Lin, L., et al. 2008, ApJ, 681, 232
Ly, C., et al. 2007, ApJ, 657, 738
Madau, P., Ferguson, H. C., Dickinson, M. E., Giavalisco, M., Steidel, C. C., Fruchter, A. 1996, MNRAS, 283, 1388
Moustakas, J., & Kennicutt, R. C., Jr. 2006, ApJS, 164, 81
Moustakas, J., Kennicutt, R. C., Jr., & Tremonti, C. A. 2006, ApJ, 642, 775
Rigopoulou, D. 2005, A&A, 440, 61
Schechter, P. 1976, ApJ, 203, 297
Takahashi, M., et al. 2007, ApJS, 172, 456
Teplitz, H. I., Collins, N. R., Gardner, J. P., Hill, R. S., & Rhodes, J. 2003, ApJ, 589, 704
Tresse, L., & Maddox, S. J. 1998, ApJ, 495, 691
Tresse, L., Maddox, S. J., Le Fevre, O., & Cuby, J. -G. 2002, MNRAS, 337, 369
Weiner, B. J., et al. 2007, ApJ, 660, L39
Willmer, C. N. A., et al. 2006, ApJ, 647, 853
Yan, L., McCarthy, P. J., Freudling, W., Teplitz, H. I., Malumuth, E. M., Weymann, R. J., & Malkan, M. a. 1999, ApJ, 519, L47

TABLE 1
OBSERVED [O II] LUMINOSITY FUNCTION

$\log L_{[\text{OII}]}$ (ergs s ⁻¹)	0.752 < z < 0.926			0.926 < z < 1.099			1.108 < z < 1.277			1.277 < z < 1.446		
	Φ	σ_{cv}	N_{gal}	Φ	σ_{cv}	N_{gal}	Φ	σ_{cv}	N_{gal}	Φ	σ_{cv}	N_{gal}
41.15	44.74 ^{+3.07} _{-2.87}	7.22	540
41.30	57.33 ^{+3.35} _{-3.17}	18.98	903	23.58 ^{+4.98} _{-4.15}	12.00	268
41.45	52.83 ^{+2.04} _{-1.97}	15.24	1065	27.58 ^{+1.70} _{-1.60}	1.81	539
41.60	44.79 ^{+1.68} _{-1.62}	7.07	1000	33.68 ^{+1.51} _{-1.44}	3.42	793	16.98 ^{+1.43} _{-1.32}	1.51	321
41.75	32.95 ^{+6.68} _{-5.61}	13.70	648	30.35 ^{+1.33} _{-1.27}	1.35	795	22.19 ^{+1.24} _{-1.17}	2.34	541	11.36 ^{+1.12} _{-1.02}	2.15	212
41.90	17.27 ^{+0.96} _{-0.91}	3.71	418	19.88 ^{+0.91} _{-0.87}	2.47	580	23.16 ^{+1.64} _{-1.53}	1.90	602	14.92 ^{+1.45} _{-1.32}	3.06	318
42.05	7.26 ^{+0.67} _{-0.61}	1.49	167	11.44 ^{+0.71} _{-0.67}	1.22	339	16.05 ^{+0.92} _{-0.87}	0.57	468	16.71 ^{+2.09} _{-1.86}	1.24	393
42.20	4.52 ^{+0.55} _{-0.49}	1.61	101	5.75 ^{+0.73} _{-0.65}	0.36	150	9.61 ^{+0.61} _{-0.57}	1.12	307	8.55 ^{+0.68} _{-0.63}	0.64	250
42.35	1.61 ^{+0.34} _{-0.28}	0.50	35	2.52 ^{+0.45} _{-0.38}	0.79	71	4.48 ^{+0.43} _{-0.40}	1.20	141	4.88 ^{+0.45} _{-0.41}	0.83	158
42.50	0.95 ^{+0.39} _{-0.28}	0.36	18	1.04 ^{+0.50} _{-0.35}	0.30	22	2.31 ^{+0.34} _{-0.30}	0.64	69	3.39 ^{+0.44} _{-0.39}	0.34	108
42.65	0.18 ^{+0.14} _{-0.08}	0.10	4	0.75 ^{+0.21} _{-0.17}	0.29	21	1.06 ^{+0.24} _{-0.20}	0.32	33	1.66 ^{+0.27} _{-0.24}	0.46	53
42.80	0.18 ^{+0.20} _{-0.10}	0.22	3	0.26 ^{+0.13} _{-0.09}	0.17	8	0.26 ^{+0.12} _{-0.08}	0.11	9	0.74 ^{+0.19} _{-0.15}	0.25	24
42.95	0.27 ^{+0.15} _{-0.10}	0.12	7	0.06 ^{+0.08} _{-0.04}	0.06	2	0.37 ^{+0.20} _{-0.14}	0.23	9	0.46 ^{+0.16} _{-0.12}	0.15	15
43.10	0.08 ^{+0.12} _{-0.05}	0.09	2	0.15 ^{+0.12} _{-0.07}	0.08	4	0.16 ^{+0.11} _{-0.07}	0.11	5	0.12 ^{+0.10} _{-0.06}	0.11	4
43.25	0.06 ^{+0.08} _{-0.04}	0.08	2	0.07 ^{+0.09} _{-0.04}	0.06	2	0.17 ^{+0.11} _{-0.07}	0.11	6
43.40	0.04 ^{+0.09} _{-0.03}	0.08	1	0.04 ^{+0.08} _{-0.03}	0.05	1	0.12 ^{+0.09} _{-0.06}	0.07	4
43.55	0.03 ^{+0.07} _{-0.02}	0.06	1	0.03 ^{+0.06} _{-0.02}	0.05	1	0.15 ^{+0.18} _{-0.09}	0.21	3
43.70	0.02 ^{+0.06} _{-0.02}	0.06	1
43.85	0.03 ^{+0.08} _{-0.03}	0.04	1	0.03 ^{+0.07} _{-0.02}	0.04	1

NOTE. — Φ is in units of $10^{-4} \text{ dex}^{-1} \text{ Mpc}^{-3}$, σ_{cv} is the 1σ uncertainty in Φ due to cosmic variance, and N_{gal} is the number of galaxies in each bin. For reference, the median redshifts of the sources in each of the four redshift bins are 0.836, 1.002, 1.194, and 1.346, respectively.

TABLE 2
PARAMETERS OF THE OBSERVED [O II] LUMINOSITY FUNCTIONS

Quantity	$0.752 < z < 0.926$	$0.926 < z < 1.099$	$1.108 < z < 1.277$	$1.277 < z < 1.446$
z_{median}	0.836	1.002	1.194	1.346
N_{gal}	5338	3845	2814	1729
Age of Universe (Gyr)	6.46	5.74	5.05	4.60
α	-3.22 ± 0.10	-3.01 ± 0.07	-3.03 ± 0.08	-2.77 ± 0.12
β	-4.11 ± 0.05	-3.89 ± 0.04	-3.68 ± 0.03	-3.55 ± 0.03
$\log [\phi(L_{\text{[OII]}} > 10^{42} \text{ erg s}^{-1})]^{\text{a}}$	$-3.70^{+0.09}_{-0.12}$	$-3.55^{+0.06}_{-0.08}$	$-3.33^{+0.09}_{-0.11}$	$-3.28^{+0.04}_{-0.04}$
$\log [L_{\text{[OII]}}(\Phi = 10^{-3.5})]^{\text{b}}$	42.23 ± 0.05	42.31 ± 0.03	42.41 ± 0.03	42.47 ± 0.01
$\log [L_{\text{TO}}]^{\text{c}}$	41.68 ± 0.10	41.75 ± 0.10	$41.93^{+0.10}_{-0.20}$	$42.00^{+0.10}_{-2.00}$
$\rho_{\text{SFR}}^{\text{d}}$	$0.09^{+0.03}_{-0.02}$	$0.10^{+0.03}_{-0.02}$	$0.12^{+0.06}_{-0.03}$	$0.12^{+0.05}_{-0.02}$

^a $\phi \equiv \int_L^\infty \Phi(L) dL$ is in Mpc^{-3} .

^b $L_{\text{[OII]}}$ is in erg s^{-1} and Φ is in $\text{dex}^{-1} \text{Mpc}^{-3}$.

^c Luminosity of the turnover in the luminosity function, L_{TO} , in erg s^{-1} .

^d Star formation rate density in $\mathcal{M}_\odot \text{yr}^{-1} \text{Mpc}^{-3}$.